Journal of Geology & Geophysics

OPEN ACCESS Freely available online

Research Article

Geophysical Geometry of Fracture Zones in the Basement Rocks of the Donga Department Northwest of Benin

Yalo N[1]*, Akokponhoué BH[1], Akokponhoué NY[1], Marc YT[2], Alassane A[1], Hounton C[1] and Suanon F[1]

[1]Laboratory of Applied Hydrology (LAH), National Water Institute (NWI), University of Abomey-Calavi, Benin; [2]University Research Center of Remote Sensing (URCRS), U.F.R of Earth Sciences and Mineral Resources, University of Félix Houphouët Boigny, Ivoiry Coast

ABSTRACT

The Donga Department is located in the northwest of Benin in an area made up of crystalline and crystallophyllic basement rocks where most of the groundwater resources are found in the area of weathered and conductive fractures. The carrying out of drilling campaigns in this department are often crowned with a significant number of negative boreholes (<0.7 m^3/h) due to the poor choice of sites for drilling. The objective of this study is to use geophysical methods to identify and characterize the fractured basement areas, with a view to improving the implantations and the sustainable management of the aquifers they contain. The Electric Resistivity Tomography method was used to characterize the geometry of the fracture zones and the thickness of the weathered zone. The results showed that in the department of Donga, the thickness of the weathered zone is between 5 and 35 m and the width of the fracture zones varies from 15 to 40 m with a vertical dip and a contrast >100. The determination of the fracture zones granulometry with T_2^* values in 5 different localities of the study area are between 150 and 212, 5 ms. It emerges from this study that in the department of Donga, few fracture zones are identified by the ERT below thick weathering layers (>20 m) and that the particle size. T_2^* of the fractured zone is also a function of geology with medium-grained gneiss and coarse-grained quartzites.

Keywords: Donga; Electric Resistivity Tomography (ERT); Fractured Zone (ZF); Geophysics T_2^*; Weathered Zone (WZ)

INTRODUCTION

Groundwater is a limited and vulnerable resource, essential for life, development and the environment. In the middle of the basement rocks, discontinuous aquifers are affected by tectonic dislocations which generate zones of fractures and weathered layers. The detection of tectonic dislocations contributes to the understanding of the functioning of the underground system [1].

Most of the groundwater resources in the Donga department are contained in basement fracture reservoirs. The work of [2-5] under the same conditions in West Africa, [6,7] in Greece and [8,9] in India have proposed a hydrogeological prospecting approach. This approach makes it possible to combine geology, hydrogeology and geophysics on the one hand. To optimise aquifer prospecting, the geophysical method is adapted to the geological nature of the area and the hydrogeological structure of the aquifer to be exploited. The combination of these methods has made it possible to characterize fractured zones favorable to the establishment of boreholes in Ivory Coast [10-12], in India [9] in Burkina Faso, [13] and in Benin [14-16]. Then, the present study aims to identify the geometry of fracture zones favorable to the establishment of boreholes in the department of Donga. This study will contribute to improving prospecting of basement fracture aquifers for access to water for populations in Africa.

Geographic, geological and hydrogeological context of the Donga department

The department of Donga is located in the northwest of Benin, between 08°28' and 10°02' north latitude and between 1°20' and 2°14' east longitude in WGS84. It covers an area of 11,126 km^2 with a population of approximately 543,130 inhabitants. It has a very dense hydrographic network with a total length of the drains estimated at 7870 km, i.e. a drainage density of 1.66 km/km^2 (Figure 1a). The relief of the Donga department is represented by the digital terrain model (Figure 1b). This model shows the different elevation levels of the Donga department. There are essentially two types of relief. A rugged terrain, located in the northwest and central part, especially northwest of the village of Alfa-kpara and

***Correspondence to:** Yalo N, Laboratory of Applied Hydrology (LAH), National Water Institute (NWI), University of Abomey-Calavi, Benin, Tel: + (225) 07-592-282, E-mail: yalonicaise@yahoo.fr

Received: January 11, 2020**; Accepted:** February 3, 2020**; Published:** February 10, 2020

Citation: Yalo N, Akokponhoué BH, Akokponhoué NY, Marc YT, Alassane A, Hounton C et al. (2020) Geophysical Geometry of Fracture Zones in the Basement Rocks of The Donga Department Northwest of Benin, J Geol Geophys 9:475. 10.35248/2381-8719.20.9.475

Copyright: © 2020 Yalo N, et al. This is an open-access article distributed under the terms of the Creative Commons Attribution License, which permits unrestricted use, distribution, and reproduction in any medium, provided the original author and source are credited.

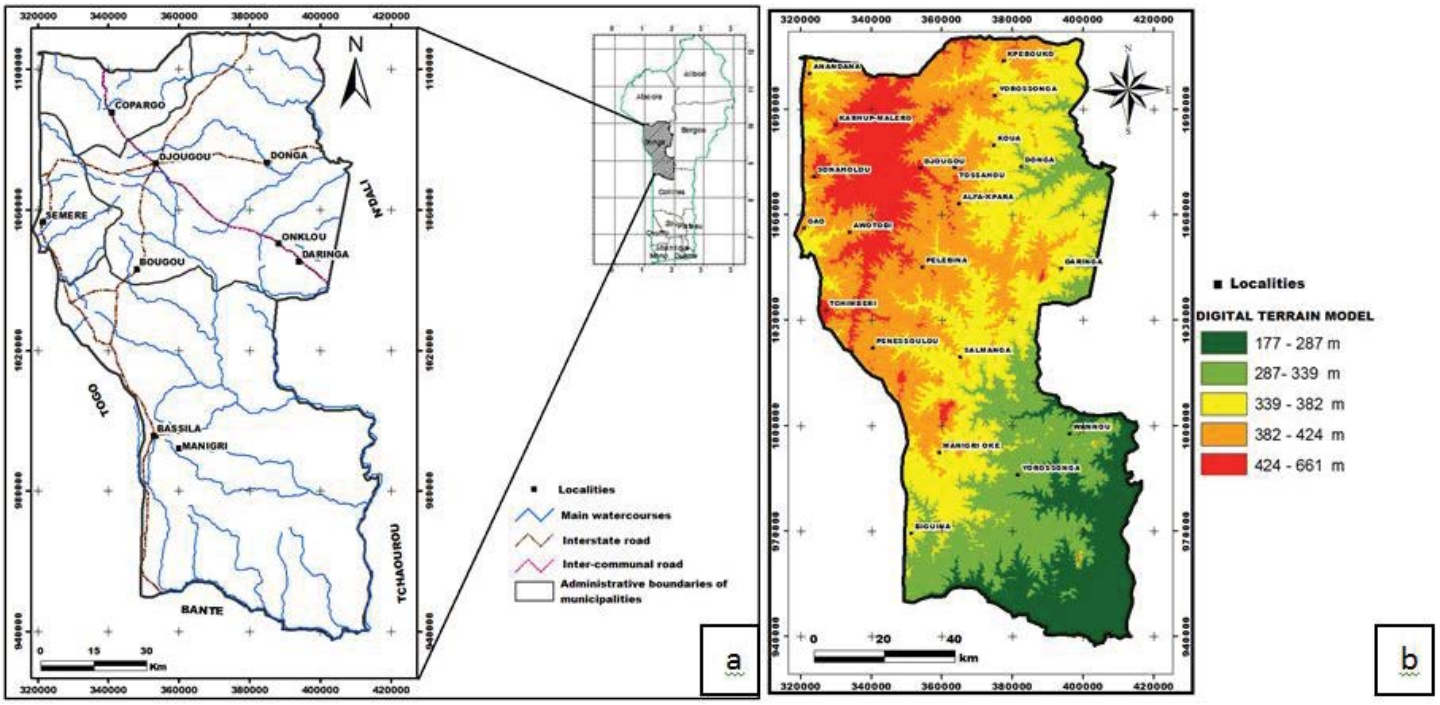

Figure 1: (a) Hydrographic chart; (b): DTM of the department of Donga.

Tanéka Koko (Mont Couffé, Mont Tanéka, Mont d'Alédjo-Koura). It is the domain of the high peaks of the Donga department where the altitudes generally exceed 660 meters. A monotonous relief, located particularly in the South-East, North-East parts, where the altitudes vary from 177 to 382 m. It is a vast, slightly inclined peneplain sharing the runoff from the Donga watersheds in the northeast and that of the Oueme watershed in the southeast. Small rivers criss-cross the peneplain in a disorderly fashion, sculpting its surface and giving it a bas-relief character.

Geologically, the study area is comprised between the outer and inner zone of the Pan-African Dahomeyides chain, comprising the structural unit of the Atacora and the structural unit of the Benin plain (Figure 2). In lithological terms, these units are respectively made up of three large ensembles (quartzites, schists and sandstones) and four large ensembles: migmatites, granulites, Mata sediments and gneisses with a high degree of metamorphism [17]; [18]. Structurally, the department of Donga has been affected by several phases of tectonic deformation, the most important of which are: the Eburnean and Pan-African orogeny (650-600 M.a.) [19]. These different events affected the territory by numerous fractures generally structured N00-20 and N20-30, the most important of which is the Kandi fault, which is a transcontinental lithospheric fracture crossing the whole territory of Benin. The work of [17,20] has shown the complexity of this zone, both locally and regionally. In addition to tectonics, other processes such as weathering, surface decompression, seismicity, etc. may favor the establishment of fracturing [21-24].

Hydrologically, there are two types of aquifers found in the study area: weathered aquifer and fractured aquifer. The first hydrogeological studies in the basement zone in Benin were carried out by [25-27] with a view to a better knowledge of the hydrogeological characteristics of this very complex environment and the possibilities of setting up wells for the water supply of the populations. During the last century, several works have increased the knowledge of the hydrogeology of the Precambrian basement rocks of West Africa and many authors [26-31] have shown that this environment contains a stock of groundwater resources likely to supply populations. Consequently, the work of [32,24] on groundwater has classically made it possible to establish different conceptual models of underground aquifers that have evolved over time. These models of aquifer structures show three main zones constituting potential reservoirs, controlled by the type of fracturing encountered: The altered layer, the fissured horizon and the hard rock (Figure 3) locally affected by geological discontinuities and deep fracturing. In this study we refer to Wyns' model and our fracture zones are located in the fissured layer just below the base of laminated layer (Figure 3).

MATERIALS AND METHODS

ERT measurements

Field measurements were performed with a Syscal R2 resistivimeter (IRIS Instruments) with Swicth 48. The length of the ERT profiles is 240 m. Ten Electrical Resistivity Tomography (ERT) panels were carried out at ten locations in the study area. The acquisition of the apparent resistivities was carried out with the dipole-dipole configuration for a spacing of 5 m between the electrodes. Synthetic modelling was carried out to represent a zone of conductive fractures (100 Ω.m) passing through a resistant basement (5000 Ω.m), under a 2 m thick layer of conductive weathering, as shown in Figure 4 in the Res2dmod software by [33].

This 8 m wide fracture zone generated a panel of apparent resistivities that were inverted in the Res2dInv software. This inverse modeling (Figure 5) provided a true resistivity model with an 8 m wide fracture zone (FZ) with resistivities ranging from 50 to 170 Ω.m and a 2 m thick weathered zone (WZ) with an average resistivity of 100 Ω.m. The ratio between the highest resistivity and the lowest resistivity (2700/50) shows that the contrast of true resistivities is greater than 20 the minimal contrast between metamorphic rock and aquifer resistivities. The Dipole-Dipole device is therefore sensitive to the detection of conductive fracture zones in the basement rocks area with precision over its width, depth and resistivity contrast.

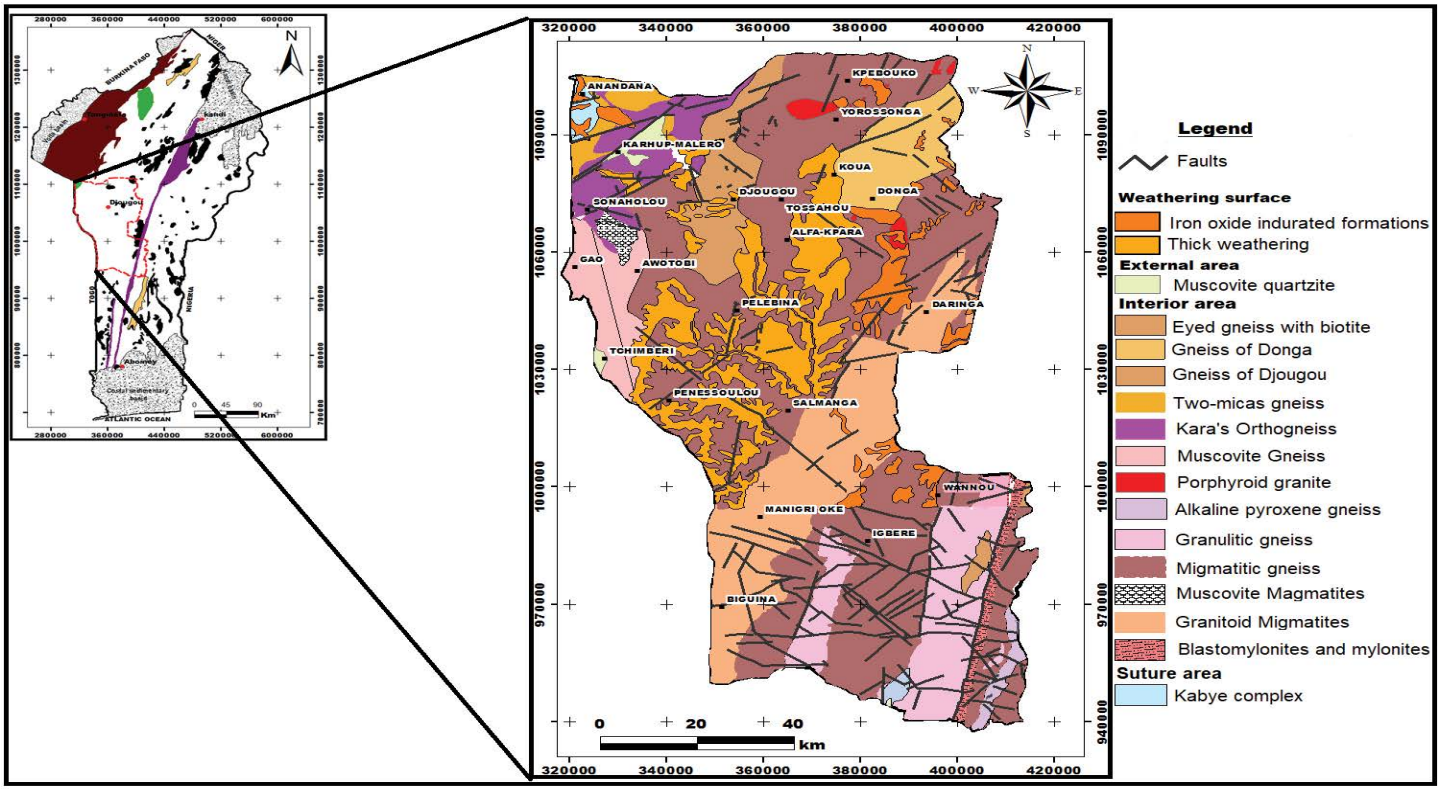

Figure 2: Geological map of the study area (modified from the geological map at 1:200000, leaf Pira-Savè; Djougou-Parakou-Nikki; Natitingou and Bembèrèkè; [19].

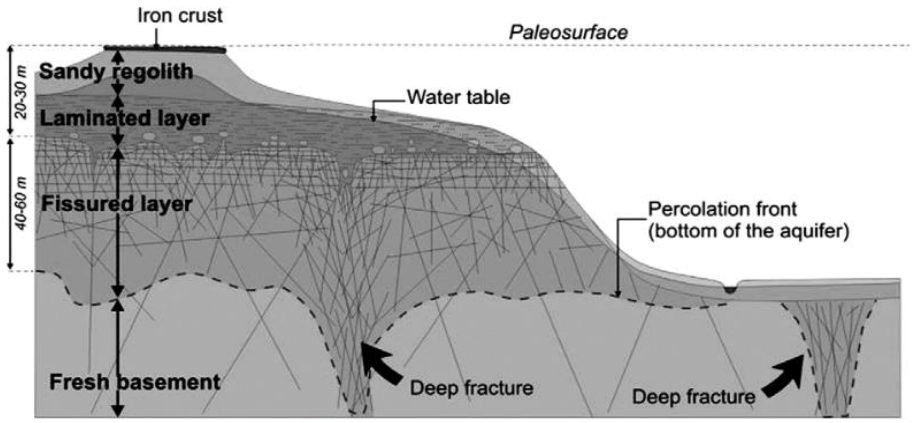

Figure 3: Conceptual model of a basement aquifer [24].

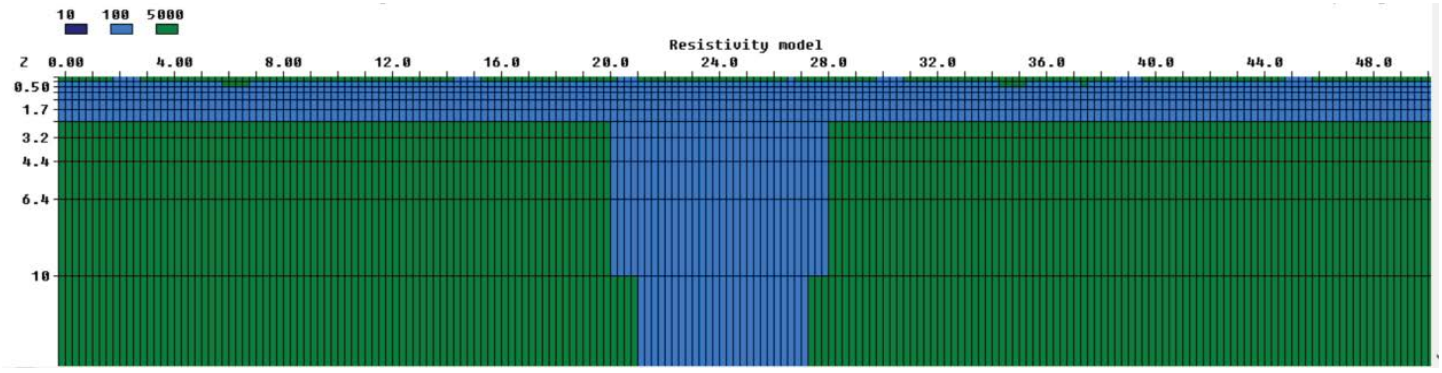

Figure 4: Direct modeling of a fracture zone.

The directions of the ERT panels vary depending on the site and the fracture zone to be validated (Table 1). The Diépani site (PS2DN) has a N-S direction (N1) and the Djougou high school site (PS8DG) is oriented NE-SW (N45). Inversion of apparent resistivity data allows reconstruction of the interpreted distribution as close as possible to the "real" distribution of resistivity in the subsurface [34]. Data inversion began with the determination of an initial model and its iterative refinement using the differences between observations and calculated responses with respect to the model parameters [34].

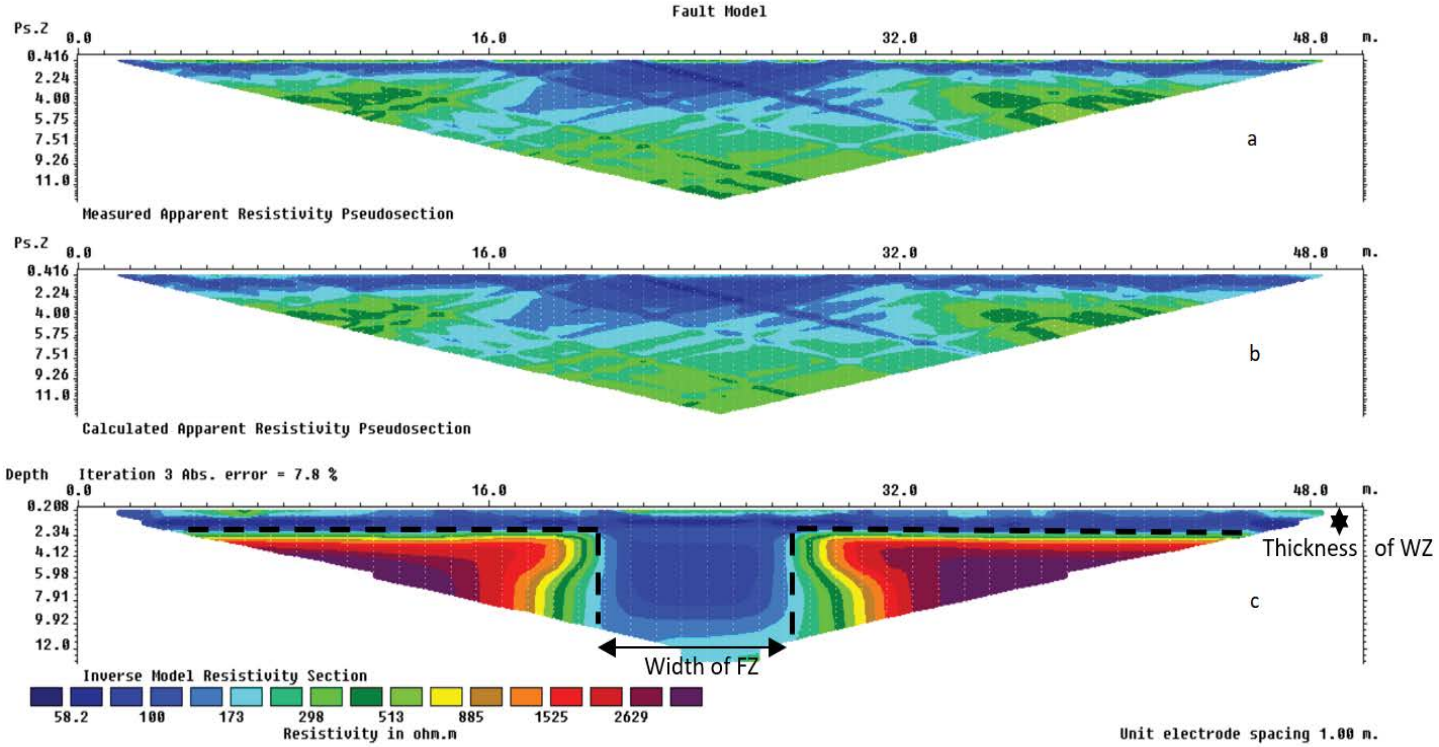

Figure 5: Fracture zone inverse modeling (a–mesured apparent resistivities, b–calculated apprent resistivities c–inverse model of true resistivities).

Table 1: Location of TRE sections.

Sites	Geological formations	Panels	Directions
Biguina II	Granitoid Migmatites	PS1BG	W-E
Diépani	Granitoid Migmatites	PS2DN	N-S
Pénéssoulou	Gneiss migmatitic	PS3PL	N-S
Bodi	Gneiss migmatitic	PS4BD	NE-SW
Pélébina	Gneiss migmatitic	PS5PN	NW-SE
Alfa kpara	Gneiss migmatitic	PS6AK	N-S
Bariénou	Gneiss migmatitic	PS7BN	NE-SW
Djougou	Gneiss of Djougou	PS8DG	NE-SW
Copargo	Quartzites	PS9CG	NE-SW
Sonaholou	Orthogneiss of Kara	PS10SL	NW-SE

T_2^* decay time constant measurements

The PMR soundings were conducted with NUMIS^{plus} RGT equipment. Generally, to implement an PMR sounding, a transmitting loop is deployed on the ground surface from which an alternating electrical current is injected. This alternating electrical current injected into the loop creates an excitation field that varies according to the Larmor frequency. This frequency is calculated after measuring the field amplitude. In fact, the implementation of an PMR survey is always conditioned by two activities. Firstly, it consists of measuring the electromagnetic noise of the site to be studied. Then, using a proton magnetometer, the ambient H_0 geomagnetic field of the site is measured. This makes it possible to determine the resonance frequency of the protons and to construct the inversion matrix of the acquired data. The size and type of loop to be deployed at a site is related to the depth to be investigated and the resistivity of the ground. Different antenna geometries (square or "8") can be used. But on a noisy site, it is advisable to use a loop in the form of an "8". This often significantly improves the signal-to-noise ratio. [35,13]. Depending on the amplitude of the electromagnetic noise, the square loop was used at two sites and the figure-of-eight loop at the other three sites (Table 2). The precise location of these five boreholes is shown in Figure 6. The characteristics of the acquisition parameters of the PMR measurements used in the department of Donga are shown in Table 2.

The NumRun acquisition software is usually used to invert PMR surveys. All the soundings in this study were conducted with fourteen pulses. Several authors [35,36] deemed it necessary to specify before any treatment that the water content (W_{PMR}) and the time constant T_2^* are not hydrogeological parameters. The signal decay time constant, T_2^*, is related to the environment in which the protons are located. The main factors that will influence this time T_2^* are the average pore size and the inhomogeneity of the static field [37]. Table 3 gives indicative T_2^* values for a few rocks: In this study, the modelling software Samovar V11.5 [38] was used to invert the data. It offers the possibility of at least qualitative interpretation of the phase of the PMR signal.

Table 2: Characteristics of PMR surveys.

Survey	Loop shape and size	Larmor frequency	Average number of stacks
S1 (Tanéka Koko)	Eight 125 m	1418 Hz	550
S2 (Donga)	Square 125 m	1413.5 Hz	130
S3 (Ara)	Eight 75 m	1412 Hz	400
S4 (Sèmèrè)	Eight 125 m	1416.8 Hz	600
S5 (Daringa)	Square 125 m	1411 Hz	250

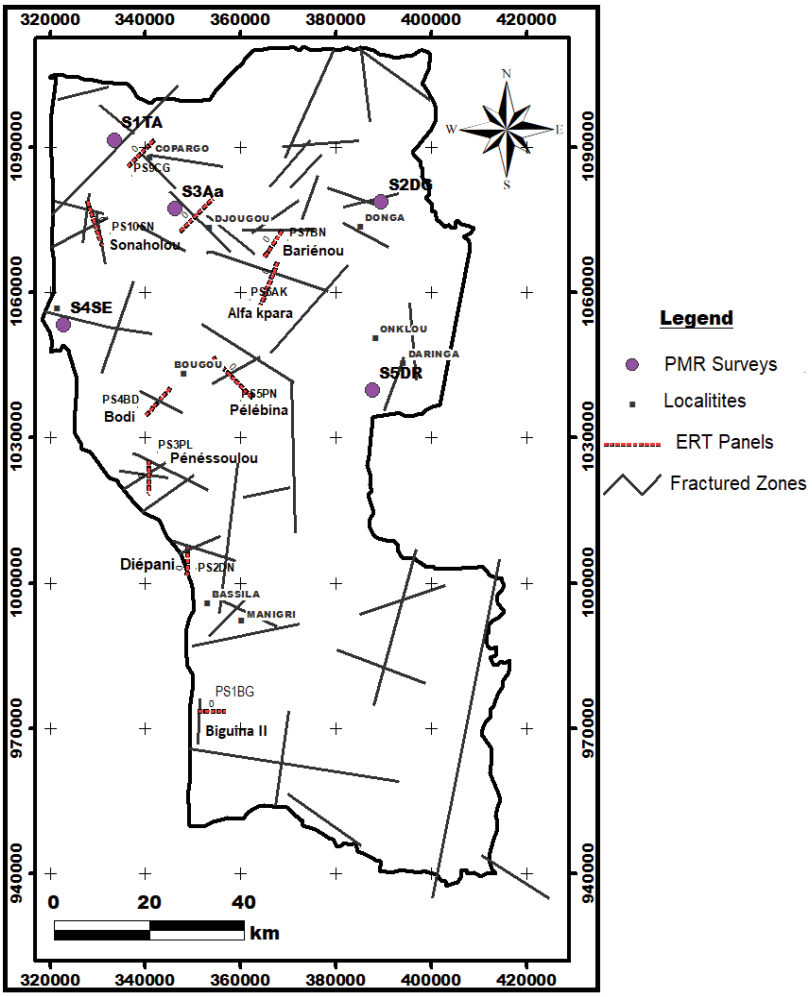

Figure 6: Location of ERT panels and PMR surveys in the study area.

Table 3: T_2^* decay time constant [37].

Types of aquifer formation	Decay time T_2^* (ms)
Sandy clay	<30
Clayey sands, very fine sand	30-60
Fine sand	60-120
Medium sands	120-180
Coarse-grained and gravelly sands	180-300
Gravel	300-600
Surface water	600-1500

RESULTS AND DISCUSSION

Contribution of the ERT to the characterization of fracture zones

Characterization of fracture zones with aquifer potential: Electrical Resistivity Tomography (ERT) provided information on the thickness of the weathered zone (WZ), the depth of the fractured zone (FZ), the weathered/bedrock (BR) resistivity contrast and the depth of the bedrock. Through 2D imaging of the subsurface, the ERT also provided information on the dip of the fractured zone. At the Diepani site, the resistivity contrast reaches 195, which shows that the resistivity of the different zones (WZ, ZFZ, BR) is quite distinct, varying between 3 Ω.m and more than 700 Ω.m. The average thickness of the weathered zone does not

exceed 10 m. The fractured zone lies between the abscissa 45 m and 85 m on the ERT section. The width of the fractured zone thus reaches 40 m and extends with a vertical dip to a depth exceeding 30 m (Figure 7).

On the Barienou site, the resistivity contrast reaches 344, which shows that the resistivity of the different zones (WZ, ZF, BR) is quite distinct, ranging from 4 Ω.m to more than 1500 Ω.m. The average thickness of the weathered zone does not exceed 10 m. The fractured zone lies between the abscissa 150 m and 170 m on the ERT section. The width of the fractured zone thus reaches 25 m but narrows with depth while extending with an oblique dip to a depth exceeding 40 m (Figure 8).

At the Bodi site, the resistivity contrast reaches 249, which shows that the resistivity of the different zones (WZ, ZF, BR) is quite distinct, ranging from 7 Ω.m to more than 1800 Ω.m. The average thickness of the weathered zone does not exceed 5 m. The fractured zone lies between the abscissa 65 m and 125 m on the ERT section. The width of the fractured zone starts at 60 m at surface and narrows to 40 m at depth where it extends with a vertical dip to the SW and oblique to the NE to a depth of less than 25 m where it meets the bedrock (Figure 9).

On the Alpha Kara site, the resistivity contrast reaches 815, which shows that the resistivity of the different zones (WZ, ZF, BR) is quite distinct, ranging from 8 Ω.m to more than 7000 Ω.m. The average thickness of the weathered zone does not exceed 8 m. The fractured zone lies between the abscissa 150 m and 170 m on the ERT section. The width of the fractured zone thus reaches 20 m and extends with a vertical dip to a depth exceeding 40 m (Figure 10). On the Pelebina site, the resistivity contrast reaches 211 which shows that the resistivity of the different zones (WZ, ZF,BS) is quite distinct, varying between 24 Ω.m and more than 5200 Ω.m. The average thickness of the weathered zone does not exceed 15 m. The fractured zone lies between the abscissa 130 m and 145 m on the ERT profile. The width of the fractured zone thus reaches 15 m and extends with a vertical dip to a depth of less than 15 m (Figure 11). A summary of these characteristics is presented in Table 4.

Characterization of the unfractured weathering layer: Electrical resistivity tomography also provides information on the absence of deep fractures despite the tectonics observed at the surface. At the Copargo site, the resistivity contrast is only 72 which show that the resistivity of the different zones (WZ, ZF, BR) is quite distinct and they vary between 141 Ω.m and more than 10000 Ω.m. The

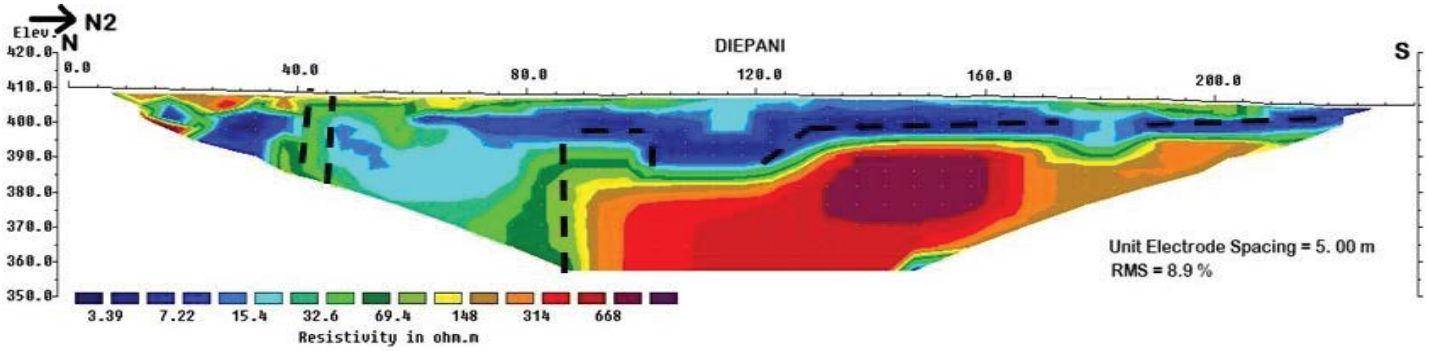

Figure 7: ERT panel of the diapeni site.

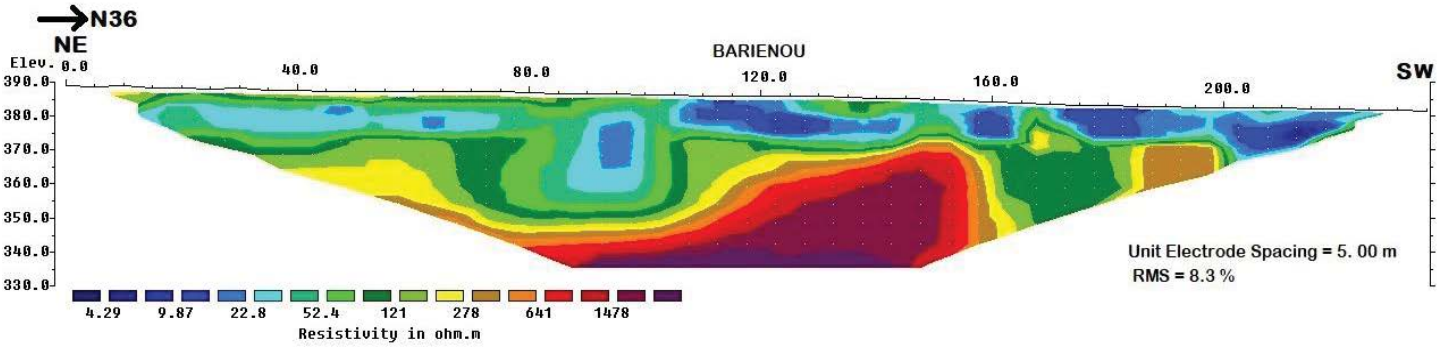

Figure 8: ERT panel of the Barienou site.

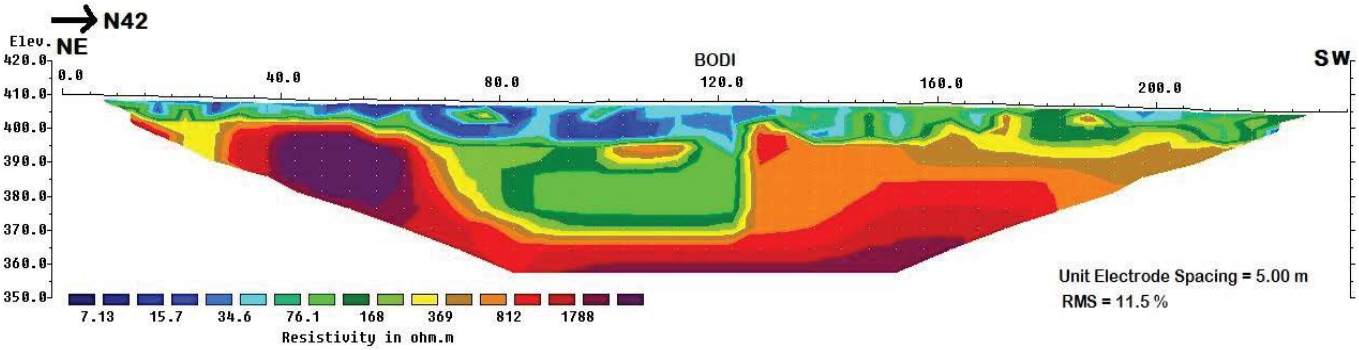

Figure 9: ERT panel of the Bodi site.

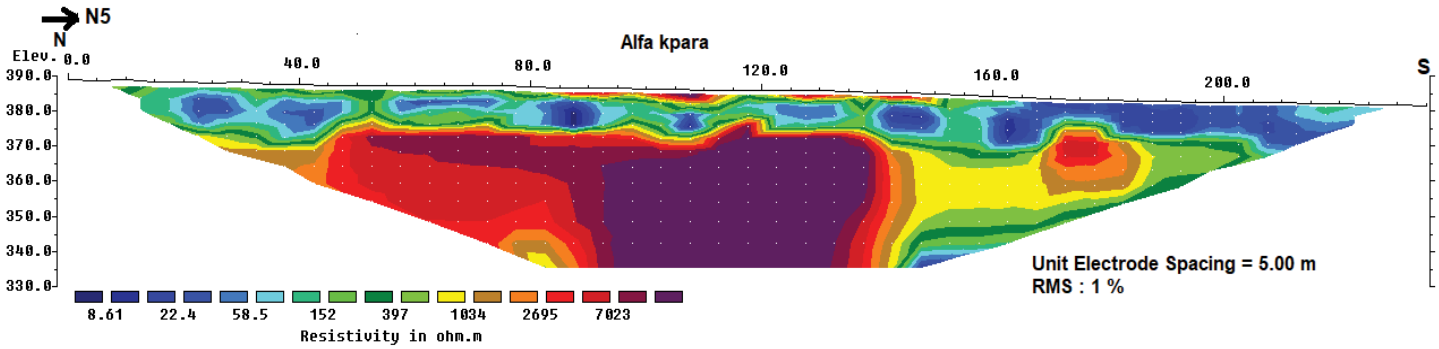

Figure 10: ERT panel of the Alpha kara site.

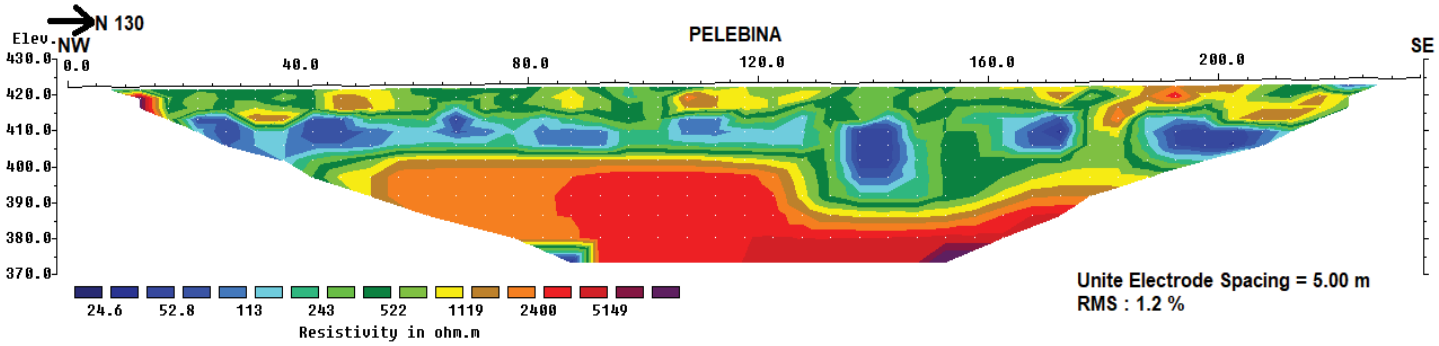

Figure 11: ERT panel of the Pelebina site.

Table 4: Geometrical characteristics of invoice areas.

Sites	Resistivity contrast	Average weathering thickness (WT)	Fracture Zone Depth (FZD)	Dip Fracture Zone (DFZ)	Fracture Zone Width (FZW)
Diépani (Bassila)	195	10 m	>30 m	Verticale	40 m
Bariénou (Djougou)	344	10 m	>40 m	Oblique	20 m
Bodi (Bassila)	249	5 m	<25 m	Verticale	40 m
Alpha Kara	815	8 m	>40 m	Verticale	20 m
Pelebini	211	15 m	<15 m	Verticale	15 m

average thickness of the weathered layer is very variable and reaches 35 m in places. No fractured zones are clearly distinct on the ERT section even though at a depth of 20 m, a 25 m wide conductor seems to be visible. The contrast in resistivity on either side of this conductor is not symmetrical (10 times weaker in the SW than in the NE), which would indicate an earlier subsidence of the weathered layer. The bedrock is located at a depth of 40 m to the NE (Figure 12). On the Penessoulou site, the resistivity contrast reaches 902 which show that the resistivity of the different zones (WZ, ZF, BR) is quite distinct with resistivities that vary between 5 Ω.m and more than 4500 Ω.m. The average thickness of the weathered layer is 23 m. No fractured zones are clearly distinct on the ERT section. The bedrock is located at a depth of 10 m to more than 35 m (Figure 13).

At the Biguina site, the resistivity contrast is only 129, which shows that the resistivity of the different zones (WZ, ZF, BR) is quite distinct, with resistivities ranging from 21 Ω.m to more than 2800 Ω.m. The average thickness of the weathered layer is 30 m. No fractured zones are clearly distinct on the ERT section. The bedrock is located at a cut depth of more than 30 m (Figure 14). A summary of the characteristics of the weathered zones is presented in Table 5.

Resistivity ranges of fractured zone's layers: According to Roques [39], the detailed description of aquifer structures through geology and geophysical imaging is an essential objective for understanding fracture reservoirs. The Dipole-Dipole (DD) type device was used in this study to validate and characterize fracture zones. Indeed, the work [15,40] carried out in a basement rock context also used this device. According to [15], the device (DD) is well suited to study geological formations and structures down to a depth of 50 m. The analysis of the ERT sections carried out shows an important variation in resistivity (4 to 10000 Ω.m) on gneisses, migmatites and granitoid migmatites. These different resistivity ranges vary according to the different layers crossed: the weathered zone (WZ) with resistivities varying from 4 to 150 Ω.m, the fractured zone (FZ) with resistivities ranging from 30 to 1000 Ω.m and a bedrock (BR) with resistivities varying from 300 to 10000 Ω.m. These resistivity ranges are slightly lower than those obtained by [15] (Figure 15). Contrary to the work of [13], the use of the ERT in the present study has made it possible to validate fracture zones. As in the crystalline basement of the department of Donga, the Dipole-Dipole device has also provided good results in several regions of the world, notably in the Armorican Massif located in the north-west of France with [39]. The use of geophysical imagery from the ERT in 10 localities in the department of Donga has also made it possible to accurately determine the thickness of the weathered zone and characterize the fractured zone crossing the bedrock basement. In fact, the average thickness of the weathered zone

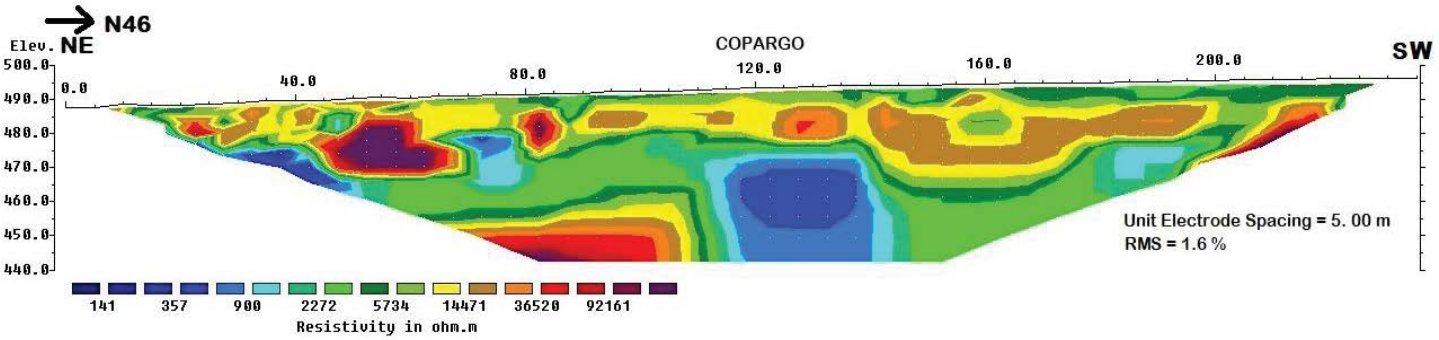

Figure 12: ERT panel of the Copargo site.

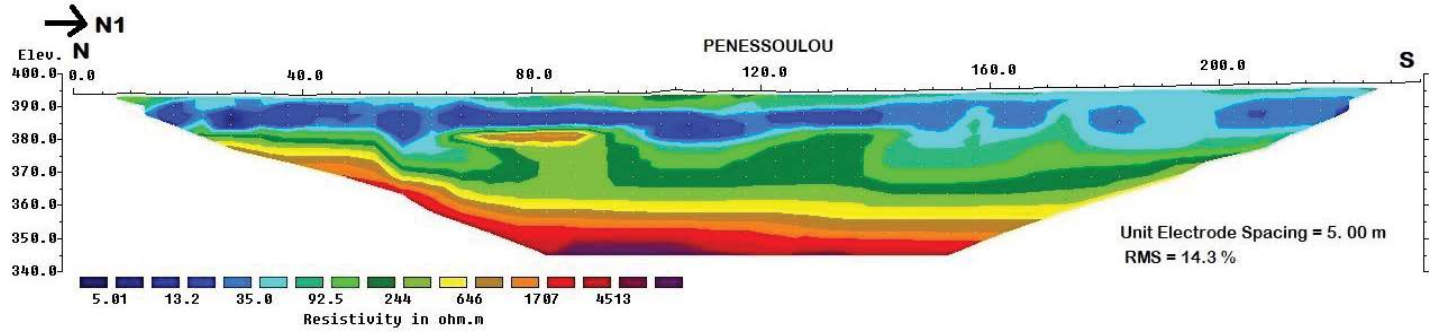

Figure 13: ERT panel of the Penessoulou site 1.

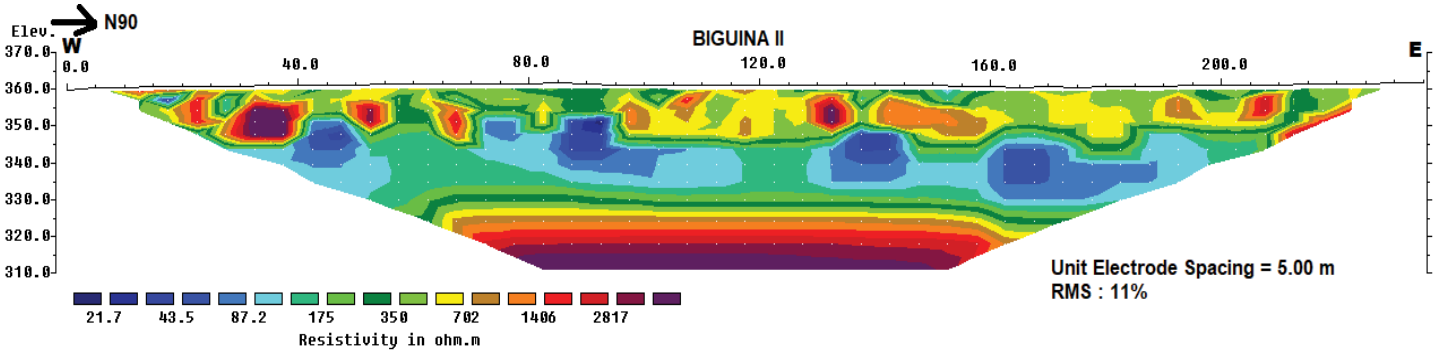

Figure 14: ERT panel of the Biguina site.

Table 5: Geometric characteristics of weathered layers.

Site	Resistivity contrast	Average weathering thickness (WT)	Bedrock Depth (BD)
Copargo	72	35 m	>35 m
Penessoulou	902	23 m	10–30 m
Biguina	129	30 m	>35 m

on all the electric panels is between 5 and 40 m. Under the most important weathering layers (>20 m), no fractures can be clearly identified. The fracture zones are more distinct under thin layers of weathering (<15 m).

Granulometry of fractured zones

The results of the five PMR surveys carried out are generally of good quality as the signal-to-noise ratios are all above 2. The lowest ratio was found in the S5DR survey with 2.2 and the highest in the S4SE survey with 12. An example of a signal-to-noise ratio of 8.3 for the PMR survey at the Ara site is shown in Figure 16.

Decay time at S1TA survey: The analysis of this survey reveals that for all the pulses, the signal is clearly free of noise. The signal amplitude at this site has the highest signal-to-noise ratio of all the soundings with 6.5. The model fits the signal well for an average noise of 11.43 nV (Figure 17). The inverted data indicate a T_2^* of 176 ms for a thickness of 24 m. In addition, the depths of the reservoir roof and impermeable bedrock are estimated as a function of static levels and bedrock depths revealed by drilling [41]. Thus, the depth of the roof is underestimated by 2.6 m by the PMR and that of the bedrock is overestimated by 10 m. The borehole depth of the fractured zone is about 45 m.

Decay time at S4SE survey: The model fits well with the data set from this survey, which has a signal-to-noise ratio of 5.16. For the other pulses, the signal is well separated from the noise. Thus, the inversion of the data indicates 171.7 ms for T_2^* for a thickness of 25 m. The average noise for this borehole is 18.28 nV, concerning, the depth of the bedrock we note that it is overestimated by 13 m

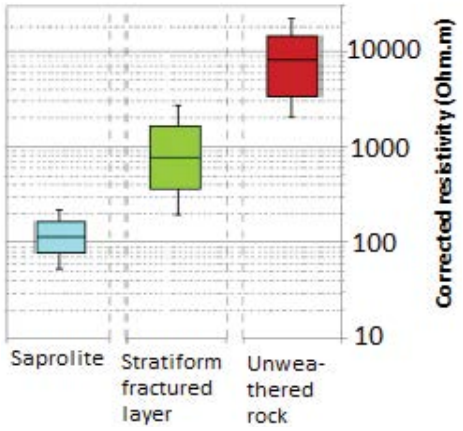

Figure 15: Resistivity ranges for WZ (saprolite), FZ (fractured layer) BR (unweathered rock) from [15].

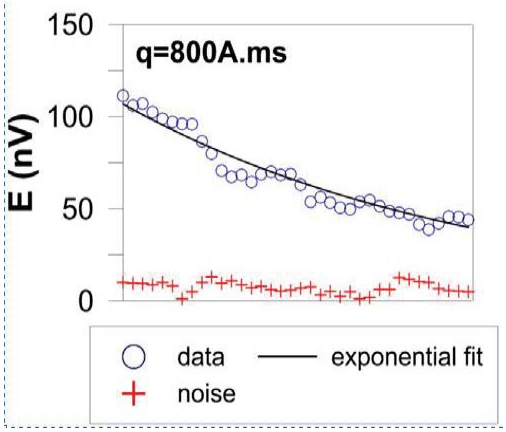

Figure 16: Signal to noise ratio (125/15) on the PMR sounding of the Ara site.

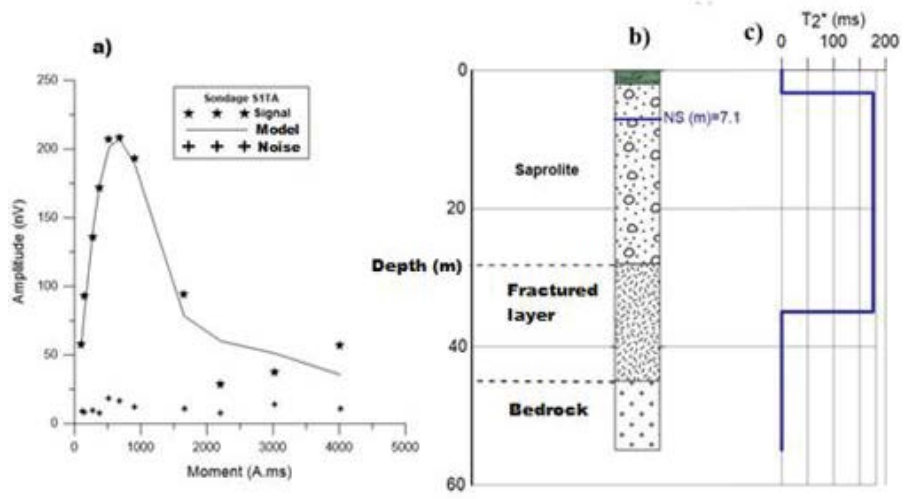

Figure 17: Presentation of PMR S1TA survey. a) Survey log b) Lithologs in the vicinity of the survey and c) Inversion decay time.

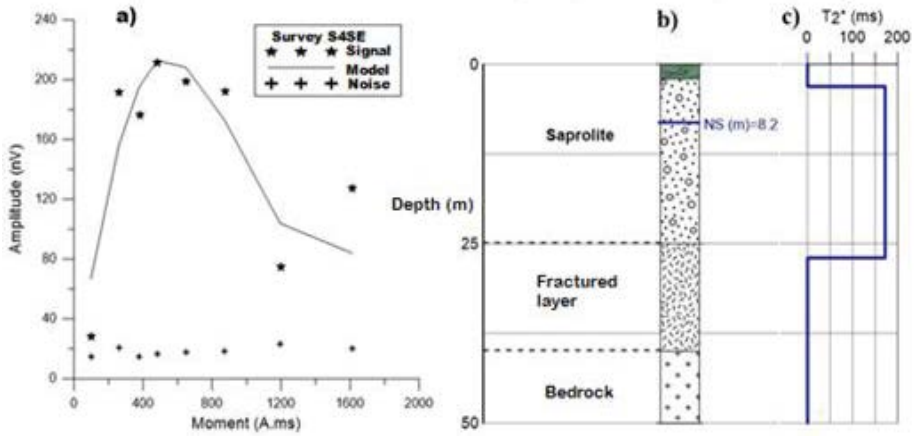

Figure 18: Presentation of PMR S4SE, a) Logs b) Lithologs in the vicinity of the borehole and c) Results of the decay time inversion.

by the borehole and that of the static level is underestimated at 2.6 m (Figure 18). The borehole depth of the fractured zone is about 40 m.

Decay time at S3ARA survey: The model fits well with the data set from this survey, which has a signal-to-noise ratio of 5.6. For the other pulses, the signal is well separated from the noise. Thus, the inversion of the data indicates 150 ms for T_2^* for a thickness of 20.5 m. The average noise for this borehole is 8 nV, concerning, the depth of the bedrock we note that it is overestimated by 18 m by the borehole and that of the static level is underestimated at 2 m (Figure 19). The borehole depth of the fractured zone is about 40 m.

Table 6 summarizes the overall results of the five PMR surveys. Indeed, these results reveal that the decay time is between 150 and 210 ms. The grain size governed by the pore size (T_2^*) is a function of the borehole thickness of the fractured zone with a correlation of 0.77 (Figure 20). The weathering with coarse sand granulometry (T_2^*=210 ms) has a fractured zone 10 m deeper than that with medium sand granulometry (T_2^*=150 ms). On S3ARA, a borehole located outside the fracture zone was found to be negative while a

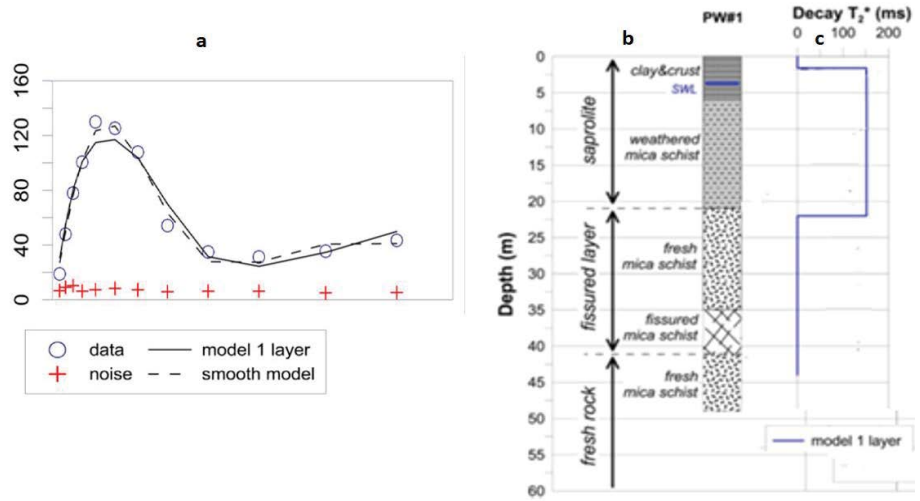

Figure 19: Presentation of the S3ARA PMR borehole, a) Logs b) Lithologs in the vicinity of the borehole and c) Results of the decay time inversion.

Table 6: Summary of T_2^* values from the PMR inversions.

Surveys	T_2^*(ms)	Thickness of FZ (m)	Geology of FZ	Signal-to-noise ratio
S1TA	176	45	Kara's Orthogneiss	6.51
S2DG	175	46	Gneiss of Donga	4.6
S3ARA	150	40	Gneiss of Djougou	5.6
S4SE	171.7	40	Granulite	5.16
S5DN	210	50	Granitoid migmatites	2.2

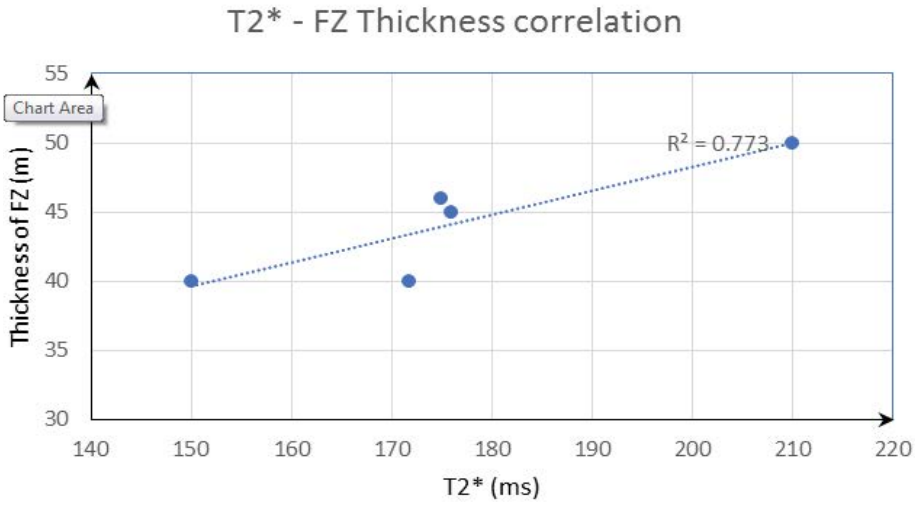

Figure 20: Relation T_2^* - FZ thickness.

second borehole located 100 m from the first and in the fracture zone was found to be positive.

The PMR decay time of the weathering layers are intimately linked to the thickness of fractured zone as well as in metamorphic rocks (gneiss) than in granitoid rocks from which they are derived. Indeed, the analysis of the results from the PMR surveys shows that the deepest fracture zones are those with the coarsest particle size. However, the geometry of the fractured zones does not depend on the geological nature of the fractured zone.

CONCLUSION

The 2D imaging of the subsurface structure resulting from the results of field investigations allows the identification of three layers: the weathering layer, the fractured zone and the bedrock. The thickness of the weathering layer varies from 6 to 40 m and that of the fractured zone is between 5 and 30 m, with variable widths between 10 and 60 m. Thus, the electrical panels carried out have revealed the position of the fracture zones likely to be aquifers, which may contribute to reducing the high failure rate in the drilling of boreholes like on S3ARA.

The analysis of the PMR surveys carried out made it possible to estimate the T_2^* values in five different localities in the study area. Indeed, the amplitudes of T_2^* are between 150 and 212.5 ms. The values of T_2^* amplitudes recorded during this study show that the weathering layers of Donga department have a coarse to medium sand grain size. The contribution of the ERT is mainly related to the detection of fracture zones with precision on their geometric properties. The contribution of the PMR is linked to the estimation of the fracture zone's granulometry which influences the depth of the fractured zone.

REFERENCES

1. Yalo Nicaise. Geological and geophysical models of the gulf of Benin and detection of tectonic dislocations in seismic data. PhD Thesis, Moscow state academy of geological prospecting (Russia) UDK 552.082.536. 2000;128.
2. Nakolendouss S, Savadogo NA, Rouleau A. The factors of productivity of crystalline basement aquifers in Burkina Faso: The example of Pobé-Mengao. 1993;95-107.
3. Saley MB. System of spatially referenced information, pseudo-image discontinuities and thematic mapping of water resources in the semi-mountainous region of Man (western Côte d'Ivoire). PhD thesis, University of Cocody. 2003;209.
4. Youan TaM, Yao KAF, Baka D, DE Lasm ZO, LASM T, Adja MG, et al. Mapping of potential zones for the implementation of high-flow drilling in fissured media by multi-criteria analysis: Case of the department of Oumé (central-western Côte d'Ivoire). J Larh. 2015;23:155-181.
5. Onetie ZO, Lasm T, Coulibaly A, Baka D, Fossou NMR, Youan TAM, et al. Contribution of GIS and multicriteria analysis in the hydrogeological prospecting of the precambrian basement of Gagnoa (Centre-Western Ivory Coast). Euro Sci J. 2016;12:137-154.
6. Antonakos A, Voudouris K, Lambrakis N. Site selection for drinking-water pumping boreholes using a fuzzy spatial decision support system in the Korinthia prefecture, SE Greece. J Hydrogeol. 2014;22:1763–1776.
7. Oikonomidis D, Dimogianni S, Kazakis N, Voudouris KA. GIS/ remote sensing based methodology for groundwater potentiality assessment in Tirnavos area, Greece. J Hydrol. 2015;525:197–208.
8. Gupta M, Srivastava PK. Integrating GIS and remote sensing for identification of groundwater potential zones in the hilly terrain of Pavagarh, Gujarat, India. Water Int. 2010;35:233–245.
9. Jhariya DC, Tarun K, Gobinath M, Prabhat D, Nawal K. Assessment of groundwater potential zone using remote sensing, GIS and multi criteria decision analysis techniques. J Geol Soci Ind. 2016;88:481-492.
10. Jourda JP. Methodology for the application of remote sensing techniques and geographic information systems to the study of fractured aquifers in West Africa, concept of spatial hydrotechnics: The case of test zones in Côte d'Ivoire. PhD thesis, University of Cocody. 2005;430.
11. Youan Ta M, Lasm T, Jourda JP, Kouame KF, Razack M. Structural mapping by ETM + satellite imagery of Landsat-7 and analysis of the networks of fractures of the Precambrian basement of the Bondoukou region (North-East of Côte d'Ivoire). Remote SM. 2008;8:119-135.
12. Youan Ta M, Lasm T, Jourda JP, Saley BM, Adja MG, Kouame K, et al. Groundwater mapping in fissured environment by multi-criteria analysis Case of Bondoukou (Ivory Coast). Int J Geo. 2011;21:43- 71.
13. Soro DD. Characterization and hydrogeological modelling of an aquifer in a fractured basement environment: case of the Sanon experimental site (central plateau region in Burkina Faso), PhD thesis, University Pierre and Marie Curie Paris. 2017;287.
14. Vouillamoz JM, Lawson FMA, Yalo N, Descloitres M. The use of magnetic resonance sounding for quantifying specific yield and transmissivity in hard rock aquifers: The example of Benin. J Appl Geophy. 2014;107:16-24.
15. Alle IC, Descloitres M, Vouillamoz JM, Yalo N, Lawson FMA, Adihou AC, et al. Why 1D electrical resistivity techniques can result in inaccurate siting of boreholes in hard rock aquifers and why electrical resistivity tomography must be preferred: The example of Benin, West Africa. J African Earth Sci. 2018;139:341-353.
16. Bertrand A. Contribution of remote sensing, geographical information systems and geophysical methods in the exploration of fracture aquifers in the Donga department (north-western Benin). PhD thesis, University of Abomey-Calavi. p. 246.
17. Affaton P. The volta basin (West Africa): A passive margin of the upper proterozoic tectonized Pan-African. State Thesis, vol 2, University Aix Marseille. 1987;462.
18. Vachette MC, Pinto KJM, Roques M. Eburnean plutons and metamorphism in the crystalline basement of the Pan-African chain in Togo and Benin. Rev Geol Dyn Phys Geog. 1979;21:351-357.
19. https://shop.geospatial.com/product/03-BJAA-Benin-200000-Geological-Maps
20. Boussari WT. Contribution to the geological study of the crystalline basement of the Pan-African mobile zone (central region of Dahomey), PhD thesis, University of Besançon. 1975:105.
21. Lasm T, Youan Ta M, Baka D, Lasme O, Jourda JP, Kouame FK, et al. Fractures networks organization on Precambrian basement of Côte d'Ivoire: Statistical and geostatistical approaches. Int Emerg Technol Adv Eng. 2014;4:1-10.
22. Lachassagne P, Wyns R, Dewandel B. The fracture permeability of hard rock aquifers is due neither to tectonics, nor to unloading, but to weathering processes. Terra Nova. 2011;23:145-161.
23. Dewandel B, Lachassagne P, Wyns R, Maréchal JC, Krishnamurthy NS. A generalized 3-D geological and hydrogeological conceptual model of granite aquifers controlled by single or multiphase weathering. J Hydrol. 2006;330:260-284.
24. Wyns R, QUEsnel F, CoinCon SR, Guillocheau F, Lacquement F. Major weathering in France related to lithospheric deformation. J Geol Fr. 2003:79-87.
25. Langsdorf W. Possibilities of groundwater exploitation in weathered schistose and crystalline structures in Dahomey/West Africa. 1971;4:82.
26. Boukari M. Contribution to the hydrogeological study of the basement regions of intertropical Africa: the hydrogeology of the Dassa-Zoumè region (Benin). PhD thesis, University of Dakar. 1982;173.
27. Boukari M, Akiti TT, Assoma D. The hydrogeology of West Africa: Synthesis of the knowledge of ancient crystalline and crystallophyllitic and sedimentary basement. 2nd Edn. 1984;147.
28. Savadogo AN. Geology and hydrogeology of the crystalline basement of Upper Volta. Regional study of the Sissil catchment area. thesis doctorate, University Grenoble. 1984;350.
29. Biemi J. Contribution to the geological, hydrogeological and remote sensing study of sub-Sahelian catchments of the precambrian basement of West Africa: Hydrostructural, hydrodynamic, hydrochemical and isotopic studies of discontinuous aquifers of furrows and granitic areas of the haute marahoué (Côte d'Ivoire). PhD thesis, University Abidjan. 1992;493.
30. Kouame KF. Hydrogeology of discontinuous aquifers in the semi-mountainous region of Man-Danané (Western Côte d'Ivoire): Contribution of satellite image data and statistical and fractal methods to the development of a spatially referenced hydrogeological information system. 3rd cycle thesis, University Cocody Abidjan, (Ivory Coast). 1999;194.
31. Lasm T. Hydrogeology of fractured basement reservoirs: Statistical and geostatistical analyses of fracturing and hydraulic properties, application to the mountain region of Côte d'Ivoire (archean domain). single PhD thesis, University of Poitier. 2000;272.
32. CIEH. Use of geophysical methods to search for water in discontinuous aquifers. BURGEAP report R.543/E. BRGM, France. 1984.

33. Loke MH, Dahlin T. A comparison of the gauss-newton and quasi-newton methods in resistivity imaging inversion. J Appl Geophy. 2002;49:149-62.

34. Olayinka AI, Yaramanci U. Assessment of the reliability of 2D inversion of apparent resistivity data. Geophy Prospec. 2000;48:293-316.

35. Boucher M. Estimation of the hydrodynamic properties of aquifers by proton magnetic resonance in different geological contexts, from sample to hydrogeological scale. PhD thesis, university of Orleans, France.2007;199.

36. Chalikakis K. Application of geophysical methods for recognition and protection of water resources in karst environments. PhD thesis, Pierre and Marie Curie University, France. 2006;212.

37. Schirov M, Legchenko A, Creer G. A new direct non-invasive groundwater detection technology for Australia. Explor Geophy. 1991;22:333-338.

38. Legchenko A, Ezersky M, Girard JF, Baltassat JM, Boucher M, Camerlynck C, et al. Interpretation of magnetic resonance soundings in rocks with high electrical conductivity. J Appl Geophy. 2008;66:118-127.

39. Roques C. Hydrogeology of crystalline basement fault zones: Implications in terms of water resources for the Armorican Massif. PhD thesis, University of Rennes. 2013;285.

40. Descloitres M, Ruiz L, Sekhar M, Legchenko A, Braun JJ, Mohan Kumar MS, et al. Characterization of seasonal local recharge using electrical resistivity tomography and magnetic resonance sounding. Hydrol Process Int J. 2008;22:384-394.

41. Vouillamoz JM. Aquifer characterization by a non-invasive method: Proton magnetic resonance soundings. PhD thesis, University Paris Sud, France. 2003;236.